Pure & Appl. Chem., Vol. 59, No. 10, pp. 1269–1284, 1987.
Printed in Great Britain.

Raman scattering by diluted magnetic semiconductors

S. Rodriguez and A. K. Ramdas

Department of Physics, Purdue University, West Lafayette, IN 47907 USA

Abstract - Raman scattering provides significant information on the nature of the magnetic excitations of diluted magnetic semiconductors (DMS). Transitions involving an exchange of a quantum of angular momentum between the system and the radiation field result in Raman lines with shifts equal to the energy of the magnetic excitations in which the total spin of the crystal changes by $\hbar$. Such transitions have a one-to-one correspondence with those seen in magnetic resonance but observed in the optical rather than in the microwave region of the electromagnetic spectrum. In the Mn-based II-VI DMS a variety of magnetic excitations have been observed in their Raman spectra. Microscopic models underlying these phenomena provide powerful insights into the nature of the magnetism of DMS.

INTRODUCTION

A semiconductor AB where A and B are, respectively, group II and VI elements, upon being alloyed with a compound MB where M is an element of the iron group, forms part of a class of materials usually called diluted magnetic semiconductors (DMS). If x is the atomic concentration of M atoms replacing atoms of type A, the formula of a DMS is written $A_{1-x}M_xB$. A typical example is $Cd_{1-x}Mn_xTe$ which can form homogeneous solid solutions for x ranging from 0 to 0.75. These materials have a unique combination of semiconducting and magnetic properties. $Cd_{1-x}Mn_xTe$ crystallizes in the zinc-blende structure for $0 \leq x \leq 0.75$ in which at random cation sites Cd is replaced by Mn atoms. For $x < 0.17$, $Cd_{1-x}Mn_xTe$ is paramagnetic for all temperatures. If $x > 0.17$, below a critical temperature $T_c(x)$, there is a magnetically ordered phase due to antiferromagnetic coupling between neighboring Mn^{2+} ions. For example, $Cd_{1-x}Mn_xTe$ with $x = 0.75$ is in an antiferromagnetic phase below 40 K.

Raman scattering studies provide significant information on the nature of the magnetic excitations of these materials. Transitions in which a quantum of angular momentum is exchanged between the system and the radiation field give rise to Raman lines whose shifts equal the energy of the magnetic excitations in which the total spin of the material changes by $\hbar$. These transitions are in one-to-one correspondence with those observed in magnetic resonance experiments but are carried out in the optical rather than in the microwave region of the electromagnetic spectrum.

MAGNETIC EXCITATIONS

General considerations

The theory of Raman scattering by magnetic excitations is similar to that by phonons except that, because of the axial nature of the magnetic field and of the magnetization $\vec{M}$, the selection rules for Raman scattering differ from those associated with symmetric polarizability tensors.

In a magnetic system, the electric susceptibility $\underline{\chi}$ is a functional of the magnetization $\vec{M}$ as well as of the other variables describing internal modes of motion. Thus we write

$$\vec{P} = \underline{\chi}(\vec{M})\cdot\vec{E}_L, \tag{1}$$

where $\vec{E}_L$ is the electric field of the incident radiation and $\vec{P}$ the polarization vector.

Several microscopic mechanisms for the dependence of $\underline{\chi}$ on $\vec{M}$ can be envisioned. Magnetostriction can conceivably be one but it is likely to yield extremely small scattering cross sections. Exchange interactions with itinerant or localized electrons, having energies comparable to electrostatic interactions, are expected to be important. This suggests that the Raman features associated with magnetic excitations should exhibit strong resonance enhancement when the energy of the quantum $\hbar\omega_L$ of the exciting radiation is near the energy of an electronic transition, e.g., the direct energy gap.

The modulation of $\vec{P}$ resulting from magnetic excitations is obtained from a Taylor series expansion of the functional $\underline{\chi}(\vec{M})$. We write

$$\vec{P} = \vec{P}^{(0)} + \vec{P}^{(1)} + \vec{P}^{(2)} + \ldots, \tag{2}$$

where the successive terms are independent of $\vec{M}$, linear in $\vec{M}$, second order in $\vec{M}$, ... The restriction imposed by the Onsager reciprocity relations, the lack of absorption in the frequency region of interest and the cubic symmetry require that (ref. 1)

$$\vec{P}^{(1)} = iG\vec{M} \times \vec{E}_L, \tag{3}$$

where G is a constant. The scattering cross section for a Raman process is proportional to

$$|\hat{\varepsilon}_S \cdot \ddot{\vec{P}}|^2$$

where $\hat{\varepsilon}_S$ is the direction of polarization of the scattered radiation. Thus the scattering cross section involving a magnetic excitation in first order is of the form

$$\sigma = C|(\hat{\varepsilon}_S \times \hat{\varepsilon}_L)\cdot\vec{M}|^2, \tag{4}$$

where $\hat{\varepsilon}_L = \vec{E}_L/|\vec{E}_L|$ is the polarization of the incident field and C is an appropriate function of ω_L and ω_S, the angular frequencies of the incident and scattered rays, respectively. Thus Raman scattering does not occur when the polarizations of the incident and scattered radiation are parallel. In the presence of a magnetic field $\vec{H}$, $\vec{M}$ varies according to the Bloch equation

$$\frac{d\vec{M}}{dt} = \gamma\vec{M} \times \vec{H}, \tag{5}$$

γ being the gyromagnetic ratio, i.e., the ratio of the magnetic-moment and the angular-momentum densitites. For electrons, $\gamma = -ge/2mc$ is negative. Considering only inelastic scattering, we need only keep the time-dependent components of $\vec{M}$. The solutions of Eq. 5, taking $\vec{H}$ parallel to the z-axis, are such that

$$M_x \pm iM_y$$

vary as $\exp[\mp i\gamma Ht]$, respectively. Since M_z and M^2 are constants of the motion, we can write

$$\vec{M} = (M_\perp \cos \Omega t,\ M_\perp \sin \Omega t,\ M_{||}), \tag{6}$$

where

$$\Omega = -\gamma H \tag{7}$$

is the Larmor frequency and $M_\perp$ and $M_{||}$ the components of $\vec{M}$ normal to and parallel to $\vec{H}$, respectively.

We consider incident radiation propagating parallel to the z-axis selected along $\vec{H}$. For circularly polarized radiation $\hat{\sigma}_+$ and $\hat{\sigma}_-$ we write

$$\vec{E}_L = (\hat{x} \pm i\hat{y})E_o \exp[-i\omega t]. \tag{8}$$

Using Eq. 3, we obtain

$$\vec{P}^{(1)} = \mp\hat{z}GM_{\perp}E_o \exp[-i(\omega \mp \Omega)t]. \tag{9}$$

This shows that in this geometry there is a Stokes line with polarization $(\hat{\sigma}_+,\hat{z})$ and an anti-Stokes line with $(\hat{\sigma}_-,\hat{z})$.

In a similar way, if the incident wave propagates at right angles to $\vec{H}$ but is polarized along $\vec{H}$,

$$\vec{E}_L = E_o\hat{z} \exp[-i\omega t] \tag{10}$$

and

$$\vec{P}^{(1)} = \frac{1}{2} GM_{\perp}E_o[(\hat{x} - i\hat{y}) \exp[-i(\omega - \Omega)t] - (\hat{x} + i\hat{y}) \exp[-i(\omega + \Omega)t]]. \tag{11}$$

Thus Stokes and anti-Stokes lines occur in the geometries $(\hat{z},\hat{\sigma}_-)$ and $(\hat{z},\hat{\sigma}_+)$, respectively. The two cases described above are, of course, related to one another by time reversal symmetry.

In order to describe the magnetic excitations observed in Raman scattering in terms of microscopic models, it is useful to consider the Hamiltonian of the Mn^{2+} ions interacting with one another and with either band electrons or electrons bound to donors. We designate the spin of a Mn^{2+} ion at the site $\vec{R}_i$ by $\vec{S}_i$ and the spin of the electron by $\vec{s}$. In the presence of a magnetic field $\vec{H}$, the Zeeman energies of the Mn^{2+} ion and of the electron are $g\mu_B\vec{H}\cdot\vec{S}_i$ and $g^*\mu_B\vec{H}\cdot\vec{s}$ where μ_B is the Bohr magneton and g and g* are the Landé g-factors of Mn^{2+} and the electron, respectively. In addition there are exchange interactions between Mn^{2+} ions at $\vec{R}_i$ and $\vec{R}_j$ of the form $-2J_{ij}\vec{S}_i\cdot\vec{S}_j$ and between an electron and the Mn^{2+} ions. The Hamiltonian of an electron in mutual interaction with Mn^{2+} ions is

$$H = -\alpha \sum_i \vec{S}_i\cdot\vec{s}|\psi(\vec{R}_i)|^2 + g^*\mu_B\vec{H}\cdot\vec{s} + g\mu_B\vec{H}\cdot\Sigma\vec{S}_i - 2\sum_{i<j} J_{ij}\vec{S}_i\cdot\vec{S}_j. \tag{12}$$

Here $\psi(\vec{R}_i)$ is the electronic wavefunction normalized over the primitive cell and evaluated at $\vec{R}_i$; αN_o is the s-d exchange integral, N_o being the number of primitive cells per unit volume.

PARAMAGNETIC PHASE

We now consider Raman transitions between Zeeman sublevels of the individual Mn^{2+} ions in an external magnetic field, the sample being in its paramagnetic phase. In this phase the exchange interaction between Mn^{2+} ions is smaller than the thermal energy k_BT and the ions can be considered as being independent of one another. The $^6S_{5/2}$ ground state of the Mn^{2+} ion has a total spin S = 5/2, orbital angular momentum L = 0 and total angular momentum J = 5/2. In this section we will discuss $Cd_{1-x}Mn_xTe$ as an illustrative example. The cubic crystalline field (site symmetry T_d) splits the sixfold degenerate ground state into a Γ_8 quadruplet state at +a, and a Γ_7 doublet at -2a, where 3a is the crystal field splitting. From electron paramagnetic resonance (EPR) experiments, Lambe and Kikuchi (ref. 2) obtained $3a = 0.0084\ cm^{-1}$ for Mn^{2+} in CdTe. This crystal field splitting is too small to be observed with the resolution of a standard Raman spectrometer and we treat the ground state of Mn^{2+} in $Cd_{1-x}Mn_xTe$ as an atomic $^6S_{5/2}$ level. The application of an external magnetic field, $\vec{H}$, results in the removal of the sixfold degeneracy of the ground state, the energy levels being $E(m_s) = g\mu_BHm_s$. Here m_s, the projection of $\vec{S}$ along $\vec{H}$, has the values -5/2, -3/2, ..., +5/2. These energy levels form the Zeeman multiplet of the ground state of Mn^{2+}.

In the paramagnetic phase, Raman scattering associated with spin-flip transitions between adjacent sublevels of this multiplet has been observed by Petrou et al. (ref. 3). The results in $Cd_{1-x}Mn_xTe$ are shown in Fig. 1 for x = 0.03. As can be seen, a strong Stokes/anti-Stokes pair is observed with a Raman shift of ω_{PM} = 5.62 ± 0.02 cm^{-1} at 40 K and H = 60 kG. Taking $\vec{H}$ and incident light parallel to $\hat{z}$ and denoting light polarization with positive and negative helicity $\hat{\sigma}_+$ and $\hat{\sigma}_-$, respectively, the Stokes line is observed in the $(\hat{\sigma}_+,\hat{z})$ configuration, whereas the anti-Stokes line is seen in $(\hat{\sigma}_-,\hat{z})$. When the incident light propagates at right angles to $\vec{H}(\hat{z})$, the Stokes component appears in the polarization $(\hat{z},\hat{\sigma}_-)$, while the anti-Stokes is observed in $(\hat{z},\hat{\sigma}_+)$. Within experimental error the frequency shift is linear in H. With the energy separation between adjacent sublevels of the Zeeman multiplet given by $\Delta E = g\mu_B H = \hbar\omega_{PM}$, it is found that g = 2.01 ± 0.02. The Raman line at ω_{PM} in $Cd_{1-x}Mn_xTe$ has been observed for a variety of compositions ranging from x = 0.01 to x = 0.70. The Raman lines labeled "SF" in Fig. 1 will be discussed in the section on SPIN-FLIP RAMAN SCATTERING.

Following the arguments given by Fleury and Loudon (ref. 4) one can consider, as a possible mechanism for the ω_{PM} Raman line, a two step process having as the intermediate state one of the excited states of the Mn^{2+} ion (L = 1, S = 5/2). For the Stokes component an incident photon of energy $\hbar\omega_L$ and polarization $\hat{\sigma}_+$ induces a virtual electric dipole transition between an initial and an intermediate state which differ by $\Delta m_J = +1$; it is followed by a second electric dipole transition between the intermediate and final states with $\Delta m_J = 0$. This is accompanied by the emission of a scattered photon of polarization $\hat{z}$ and energy $\hbar\omega_S = \hbar\omega_L - \hbar\omega_{PM}$. At the end of this process the Mn^{2+} ion is in an excited state within the Zeeman multiplet differing from the initial state by $\Delta m_S = +1$. There is also a Stokes component in the $(\hat{z},\hat{\sigma}_-)$ configuration. Similar processes can be visualized for the anti-Stokes component having the $(\hat{\sigma}_-,\hat{z})$ or the $(\hat{z},\hat{\sigma}_+)$ polarization. This mechanism correctly predicts the experimentally observed polarization characteristics of the Stokes and anti-Stokes components of the ω_{PM} Raman line. We note that the selection rules are immediate consequences of conservation of angular momentum of the system comprised of the Mn^{2+} ions and the photon field. It should also be pointed out that the Stokes scattering process in the $(\hat{\sigma}_+,\hat{z})$ configuration is the time reversed conjugate of the $(\hat{z},\hat{\sigma}_+)$ anti-Stokes process; in the same manner, the $(\hat{z},\hat{\sigma}_-)$ Stokes and the $(\hat{\sigma}_-,\hat{z})$ anti-Stokes processes are related by time reversal.

Exploiting the variation of the band gap with manganese concentration and/or temperature, it is possible to match the band gap of several samples with the energy of one of the discrete lines of a Kr^+ laser. In addition, a dye laser can also be used to achieve resonant conditions. It is found that the intensity of the ω_{PM} line increases by several orders of magnitude as the laser photon energy approaches that of the band gap. The observation of this resonant enhancement in the intensity of the ω_{PM} Raman line prompts the consideration of a mechanism involving interband transitions. It involves the Mn^{2+}-band electron exchange interaction described by the first term in the Hamiltonian in Eq. 12. The term $\vec{S}_i \cdot \vec{s}$ can be written as

$$\vec{S}_i \cdot \vec{s} = S_i^{(z)} s^{(z)} + \frac{1}{2} S_i^{(+)} s^{(-)} + \frac{1}{2} S_i^{(-)} s^{(+)}; \tag{13}$$

here $S_i^{(\pm)}$ and $s^{(\pm)}$ are the spin raising and lowering operators for a Mn^{2+} ion and band electron, respectively, and $S_i^{(z)}$ and $s^{(z)}$ are the corresponding projections of spin along $\hat{z}$. The second term of Eq. 13 raises the spin of a Mn^{2+} ion while simultaneously lowering the spin of a band electron, i.e.,

$$|m_S\rangle_{Mn^{2+}} |m_J\rangle_e \rightarrow |m_S + 1\rangle_{Mn^{2+}} |m_J - 1\rangle_e. \tag{14}$$

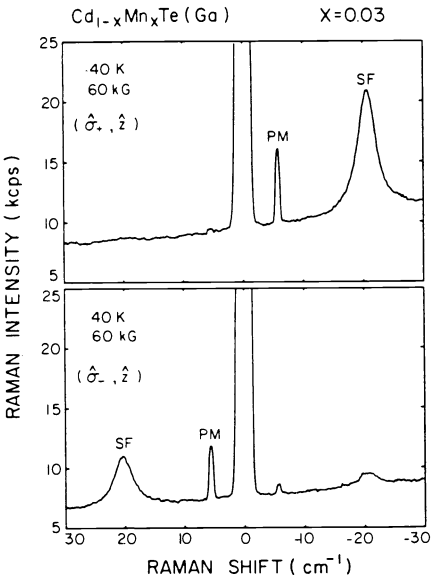

Fig. 1

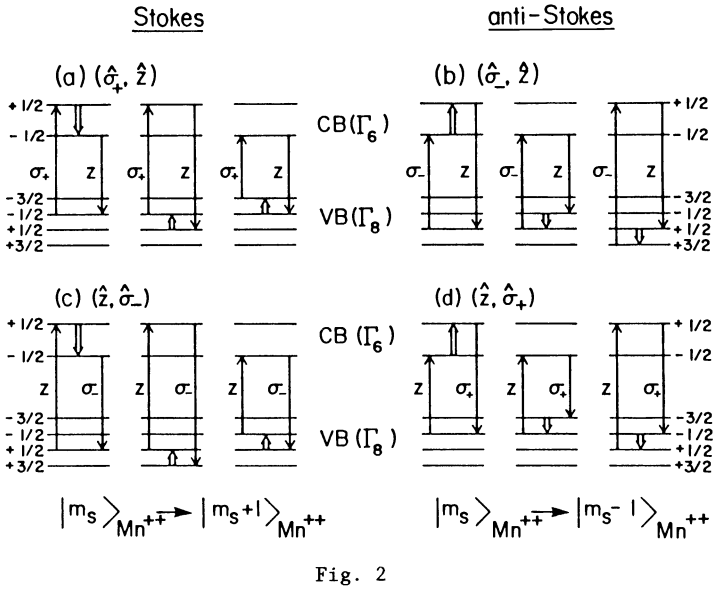

Fig. 2

Fig. 1. Raman spectra of $Cd_{1-x}Mn_xTe(Ga)$, $x = 0.03$, showing the $\Delta m_S = \pm 1$ transitions within the Zeeman multiplet of Mn^{2+} (PM) and the spin-flip of electrons bound to Ga donors (SF). kcps $\equiv 10^3$ counts/sec. (Peterson et al., ref. 29).

Fig. 2. Raman mechanism for the ω_{PM} line involving the band electrons: CB and VB refer to the conduction and valence bands, respectively, which are labeled by the electronic quantum number m_J. The single arrows indicate virtual electric-dipole transitions, while the double arrows refer to transition induced by the electron-Mn^{2+} exchange interaction. The allowed polarizations for the Stokes component are $(\hat{\sigma}_+,\hat{z})$ (a) and $(\hat{z},\hat{\sigma}_-)$ (c), while those for the anti-Stokes are $(\hat{\sigma}_-,\hat{z})$ (b) and $(\hat{z},\hat{\sigma}_+)$ (d) (Petrou et al., ref. 3).

In a similar fashion, the third term lowers the spin of an ion while raising the spin of a band electron, i.e.,

$$|m_S\rangle_{Mn^{2+}} |m_J\rangle_e \rightarrow |m_S - 1\rangle_{Mn^{2+}} |m_J + 1\rangle_e. \tag{15}$$

Hence, these terms can induce simultaneous spin-flips of the band electrons on the one hand and the Mn^{2+} ions on the other, corresponding to $\Delta m_S(Mn^{2+}) = \pm 1$ and $\Delta m_J(e) = \mp 1$.

In Fig. 2 we show the above mechanism for both the Stokes and the anti-Stokes component and the two right-angle geometries considered above. In the presence of a magnetic field the Γ_8 valence band splits into four subbands with $m_J = -3/2, -1/2, +1/2$, and $+3/2$, and the Γ_6 conduction band splits into $m_J = +1/2$ and $-1/2$ subbands. The possible processes for the Stokes component appearing in the $(\hat{\sigma}_+,\hat{z})$ configuration are shown in Fig. 2a. In the first process an incident photon of polarization $\hat{\sigma}_+$ is absorbed, raising an electron to the conduction band with $\Delta m_J = +1$ and creating a hole in the valence band. In the second step the excited electron interacts with a Mn^{2+} ion via the second term of Eq. 13, resulting in $\Delta m_S(Mn^{2+}) = +1$ and $\Delta m_J(e) = -1$. Finally, the electron and hole recombine emitting a photon of energy $\hbar\omega_S = \hbar\omega_L - \hbar\omega_{PM}$ of polarization $\hat{z}$; the band electrons have thus returned to their initial state, but leaving the Mn^{2+} ion excited to the next sublevel of the Zeeman multiplet. In the other two processes shown in Fig. 2a the hole, rather than the excited electron, interacts with the Mn^{2+} ion, resulting, however, in identical polarization selection rules. In the same manner the Stokes component in the $(\hat{z},\hat{\sigma}_-)$ configuration follows from Fig. 2c. The anti-Stokes processes for the $(\hat{\sigma}_-,\hat{z})$ and the $(\hat{z},\hat{\sigma}_+)$ geometries are shown in Figs. 2b and 2d, respectively.

All the observations discussed above and the predictions of the microscopic models considered are in accord with the general phenomenological selection rules embodied in Eqs. 8-11. We also note that this entire phenomenon is electron paramagnetic resonance observed as Raman shifts, i.e., it is Raman-EPR.

One can also visualize a mechanism in which the Mn^{2+}-electron and Mn^{2+}-hole exchange interactions result in a similar Raman line but with a shift of $2\omega_{PM}$. The processes resulting in a Raman shift of $2\omega_{PM}$ are shown in Fig. 3. For example, in Fig. 3a, a photon of polarization $\hat{\sigma}_+$ is absorbed, virtually exciting an electron from the $m_J = -1/2$ valence sub-band to the $m_J = +1/2$ conduction sub-band. The excited electron then interacts with a Mn^{2+} ion resulting in $\Delta m_S(Mn^{2+}) = +1$ and $\Delta m_J(e) = -1$, while the hole in the valence band interacts in the same manner yielding $\Delta m_S(Mn^{2+}) = +1$ and $\Delta m_J(e) = -1$. Figures 3b and 3c show how a Stokes shift of $2\omega_{PM}$ might arise exclusively through a Mn^{2+}-valence electron exchange interaction; from Eq. 13 it is clear that such an interaction will involve two successive Mn^{2+} spin flips. Due to the extended wavefunctions of both the conduction electron and the hole it should be more probable that this process involves two Mn^{2+} ions rather than just one. Similarly, the anti-Stokes components of the mechansim are those presented in Figs. 3d-3f. Energy conservation requires that the energy of the scattered photon be $\hbar\omega_S = \hbar\omega_L \mp 2\hbar\omega_{PM}$. The polarization selection rules predicted by this mechanism are $(\hat{\sigma}_+,\hat{\sigma}_-)$ for the Stokes and $(\hat{\sigma}_-,\hat{\sigma}_+)$ for the anti-Stokes components of the Raman line at $2\omega_{PM}$. This mechanism is expected to be significant only close to resonance.

The Raman line at $2\omega_{PM}$ has been observed under resonant conditions for a variety of compositions. The results for $Cd_{1-x}Mn_xTe$ with $x = 0.10$ are shown in Fig. 4; in this case, resonant conditions were achieved by maintaining a sample temperature of 120 K and using the 7525 Å line of the Kr^+ laser as the exciting radiation. The forward scattering geometry was used in order to obtain the $(\hat{\sigma}_+,\hat{\sigma}_-)$ and $(\hat{\sigma}_-,\hat{\sigma}_+)$ configurations. As can be seen in Fig. 4, the Stokes and the anti-Stokes lines appear with the expected polarizations. Under the resonant conditions of this experiment the ω_{PM} line is extremely intense ($\sim 10^6$ counts/sec); although this line is forbidden for these polarizations; it is not surprising that the leakage observed is quite strong.

It is known that electrons and holes in polar crystals interact strongly with zone center longitudinal optical (LO) phonons through the Fröhlich interaction (see Hayes and Loudon, ref. 5). An LO phonon can be created or annihilated as a result of such an interaction. Referring to the mechanism responsible for the ω_{PM} line one can visualize a fourth step in which the excited electron or hole interacts with the lattice and creates or annihilates an LO phonon. Such a mechanism would result in a scattered photon with a Raman shift of $\omega_{LO} \pm \omega_{PM}$. The net result for the Stokes process with a shift of $\omega_{LO} + \omega_{PM}$ is that an LO phonon is created and a Mn^{2+} ion is excited to the next sublevel of the Zeeman multiplet. A Stokes shift of $\omega_{LO} - \omega_{PM}$ corresponds to the creation of an LO phonon and the de-excitation of a Mn^{2+} ion to the next lower sublevel of the multiplet. The $\omega_{LO} + \omega_{PM}$ Stokes Raman line is expected to appear in the $(\hat{\sigma}_+,\hat{z})$ or the $(\hat{z},\hat{\sigma}_-)$ configurations, whereas the $\omega_{LO} - \omega_{PM}$ Stokes line is allowed for $(\hat{\sigma}_-,\hat{z})$ or $(\hat{z},\hat{\sigma}_+)$.

In addition to the above, the creation or annihilation of two LO phonons in a similar process is also possible. An electron or a hole can create or annihilate two LO phonons in a single step. Another possibility is that an electron as well as a hole each separately create an LO phonon. In either case, the scattered photon can have the following Raman shifts:

$$2\omega_{LO_1} \pm \omega_{PM},\ \omega_{LO_1} + \omega_{LO_2} \pm \omega_{PM} \text{ or } 2\omega_{LO_2} \pm \omega_{PM},$$

where LO_1 refers to the "CdTe-like" and LO_2 to the "MnTe-like" zone center longitudinal

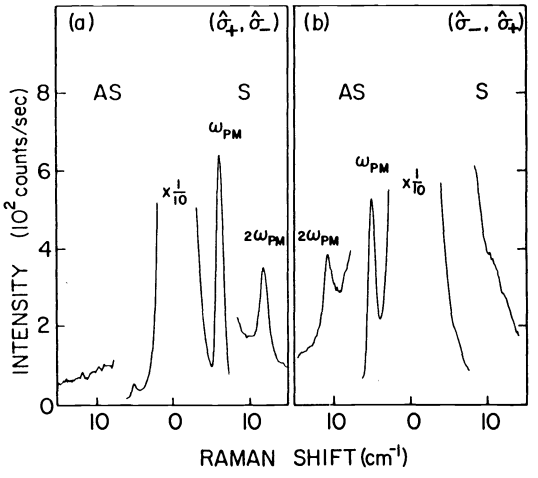

Fig. 3

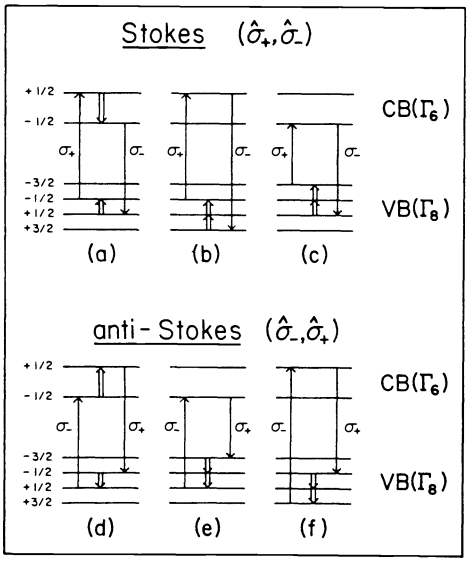

Fig. 4

Fig. 3. Raman mechanism for the $\Delta m_S = \pm 2$ spin-flip transition, i.e., the $2\omega_{PM}$ line, involving the band electrons. The Stokes line is allowed in $(\hat{\sigma}_+,\hat{\sigma}_-)$ polarization, whereas the anti-Stokes appears in $(\hat{\sigma}_-,\hat{\sigma}_+)$. (Petrou et al., ref. 3).

Fig. 4. Stokes and anti-Stokes components of $2\omega_{PM}$ in $Cd_{1-x}Mn_xTe$, x = 0.10, recorded for the $(\hat{\sigma}_+,\hat{\sigma}_-)$ and $(\hat{\sigma}_-,\hat{\sigma}_+)$ polarizations. The sample temperature T = 120 K, H = 60 kG, and λ_L = 7525 Å; x, y, and z are along [110], [$\bar{1}$10], and [001], respectively. The ω_{PM} line appearing in the spectra is due to leakage (Petrou et al., ref. 3).

optical phonons (ref. 6). As before the Stokes lines involving the excitation of a Mn^{2+} ion are expected in the $(\hat{\sigma}_+,\hat{z})$ or $(\hat{z},\hat{\sigma}_-)$ polarization geometries, while those involving a de-excitation of a Mn^{2+} ion appear in $(\hat{\sigma}_-,\hat{z})$ or $(\hat{z},\hat{\sigma}_+)$.

The new lines described above should occur only under conditions of band-gap resonance. Under such conditions we have indeed observed the new Raman lines with shifts of $\omega_{LO} \pm \omega_{PM}$ in $Cd_{1-x}Mn_xTe$ for a variety of compositions. The Raman spectra in the region of the longitudinal and transverse optical (TO) vibrational modes are shown in Fig. 5 for $Cd_{1-x}Mn_xTe$ with x = 0.10. The 7525 Å Kr^+ laser line was used to excite the spectra. The zero magnetic field LO and TO phonon spectrum is shown in Fig. 5b. Here the "CdTe-like" TO and LO and the "MnTe-like" LO modes are quite distinct, while the "MnTe-like" TO appears as a shoulder to the LO. The corresponding Raman spectra, recorded in the presence of a magnetic field of 60 kG and in the $(\hat{z},\hat{\sigma}_+)$ and $(\hat{z},\hat{\sigma}_-)$ configurations, are presented in Figs. 5a and 5c, respectively. The additional Raman lines with Stokes shifts $\omega_{LO} \pm \omega_{PM}$ are clearly present with the proper polarization characteristics. The sample temperature was 120 K; at this temperature, the sublevel occupation probability ratio of adjacent levels in the Zeeman multiplet of Mn^{2+} is $\exp(-\hbar\omega_{PM}/k_BT) = 0.94$. Thus the intensities of the $\omega_{LO} + \omega_{PM}$ and the $\omega_{LO} - \omega_{PM}$ lines are expected to be approximately equal. The $\omega_{LO} \pm \omega_{PM}$ lines can be observed only when the exciting photon energy is stronly resonant with the band gap. There is no evidence of corresponding Raman lines associated with the TO phonons, which would have shifts of $\omega_{TO} \pm \omega_{PM}$. This supports the assumption that the Fröhlich interaction is responsible for the appearance of the new features.

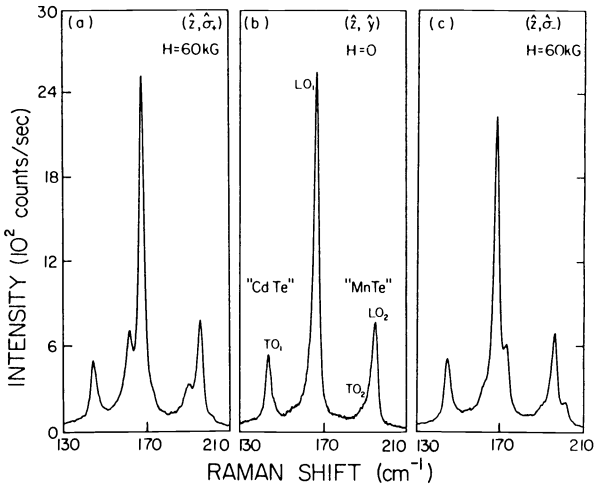

Fig. 5

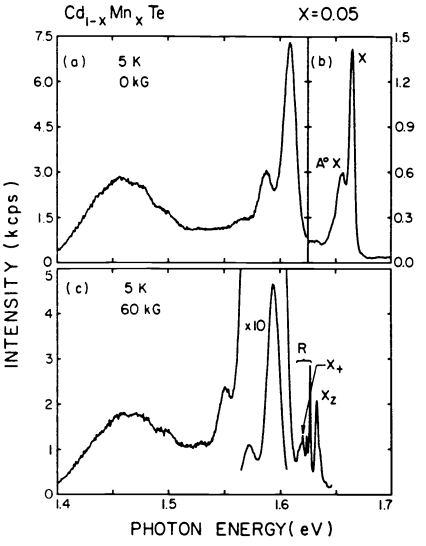

Fig. 6

Fig. 5. Raman spectra of $Cd_{1-x}Mn_xTe$, x = 0.10, showing the combination lines $\omega_{LO_1} \pm \omega_{PM}$ and $\omega_{LO_2} \pm \omega_{PM}$, where LO_1 and LO_2 are the "CdTe-like" and "MnTe-like" LO phonons. The sample temperature T = 120 K, H = 60 kG, and λ_L = 7525 Å; x, y, and z are along [110], [001], and [1$\bar{1}$0], respectively. (Petrou et al., ref. 3).

Fig. 6. The photoluminescence spectra of $Cd_{0.95}Mn_{0.05}Te$ at T = 5 K with H = 0 for (a) and (b), H = 60 kG for (c), λ_L = 7525 Å for (a) and (c), λ_L = 6764 Å for (b), and P_L = 25 mW for all cases. Raman features are denoted by 'R'. In (c) the features between 1.55 and 1.6 eV are also displayed on a scale reduced by 10. (Peterson et al., ref. 28).

The scattering amplitude for the Raman mechanism discussed above is proportional to the magnitude of the exchange coupling between the Mn^{2+} ions and the band electrons which is especially strong in these alloys. Adapting Loudon's theory (ref. 7 and 8) for optical phonons, the scattering cross section for such a three-step process can be written as being proportional to

$$\left| \frac{\langle n_S+1,0|H_{eR}|n_S,b\rangle \langle m_S+1,b|H_{ex}|m_S,a\rangle \langle n_L-1,a|H_{eR}|n_L,0\rangle}{(\omega_b + \omega_{PM} - \omega_L)(\omega_a - \omega_L)} + 5 \text{ additional terms} \right|^2. \qquad (16)$$

Here

H_{eR} = electron-photon interaction Hamiltonian,

H_{ex} = exchange Hamiltonian describing the exchange interaction between 3d-localized states of Mn^{2+} and conduction (valence) electrons,

n_L, n_S = occupation numbers of the incident and scattered photon modes, respectively,

$\hbar\omega_a, \hbar\omega_b$ = intermediate excitation energies of the virtual electron-hole pair.

The other five terms in Eq. 16 are the remaining permutations of the three steps of the Raman process. It is clear that the first term will dominate when $\omega_a \sim \omega_L$ or $\omega_b \sim (\omega_L - \omega_{PM}) = \omega_S$, producing a double peak in the frequency dependence of the cross section. The condition of "in resonance" results from the matching of the incident photon energy with that of an electronic excitation whereas "out resonance" occurs when the scattered photon energy equals the energy of such a transition (ref. 9).

In Eq. 16, $\hbar\omega_a$ and $\hbar\omega_b$ are the energies of excitation of two states of the exciton with angular momenta differing by one unit. For example, following Twardowski et al (ref. 10) for a $(\hat{z},\hat{\sigma}_+)$ Stokes line

$$\begin{aligned} \hbar\omega_a &= E_x - 3A + B, \\ \hbar\omega_b &= E_x - 3A + 3B \end{aligned} \tag{17}$$

where E_x is the exciton energy and

$$\begin{aligned} A &= \frac{1}{6}\, xN_o\alpha \langle S_z^{Mn}\rangle, \\ B &= \frac{1}{6}\, xN_o\beta \langle S_z^{Mn}\rangle. \end{aligned} \tag{18}$$

In Eq. 17, it is assumed that the electron-hole exchange and correlation energy is insensitive to $\vec{H}$. In Eq. 18 $\alpha(\beta)$ is the exchange integral of the 3d states of Mn^{2+} and conduction (valence) electrons and $\langle S_z^{Mn}\rangle$ is the average value of the component of Mn^{2+} spin along $\vec{H}$ given by (5/2) $B_{5/2}(g\mu_B H/k_B T)$ in the paramagnetic phase. Thus the energies $\hbar\omega_{a,b}$ are characterized by an effective g factor which is a nonlinear function of (H/T).

In Fig. 6, (a) and (b), we show the photoluminescence spectrum of $Cd_{1-x}Mn_xTe$, x = 0.05, at 5 K in the absence of a magnetic field. The feature labeled X is attributed to free exciton recombination (ref. 11) and has an energy of E_x = 1.665 eV, an increase of 70 meV from the value in CdTe. The energy of this exciton varies linearly with Mn^{2+} concentration (ref. 12) in $Cd_{1-x}Mn_xTe$ and the value measured here is in good agreement with that expected. The feature labeled A°X is attributed to the exciton bound to a neutral acceptor (ref. 11) with a binding energy of 9 meV. The feature at 1.608 eV, when corrected for the change in the energy gap, corresponds to the 1.54 eV feature in CdTe which may result from free electron to acceptor transitions; the features at 1.587 and 1.566 eV are the LO phonon replicas of this transition. Similarly, the series of luminescence peaks beginning at ~1.5 eV are the LO phonon replicas of the transitions assoicated with a vacancy-donor complex $(V_{Cd}^{2-}D^{+})$ where the donors in this case are presumed to be interstitial copper atoms introduced during the crystal growth. As the magnetic field is increased the free exciton peak increases in intensity and shifts to lower energy sweeping across the A°X feature (ref. 11). At sufficiently high magnetic fields a splitting in the free exciton feature is observed (ref. 13). Two of these are present in Fig. 6(c); the low energy component labeled X_+ appears in the $\hat{\sigma}_+$ polarization, while the other, X_z, is polarized along $\hat{z}$. The feature associated with the free electron to acceptor transition and its LO phonon replicas shift by 14 meV in a magnetic field of 60 kG.

On the basis of the luminescence spectra, appropriate choices of laser wavelength, sample temperature and magnetic field can be made to achieve conditions of "in resonance" or "out resonance" which can selectively enhance specific features in the Raman spectrum. In the experiments reported here, the $\omega_{LO} - \omega_{PM}$ line, i.e., the Raman shift with the creation of an LO phonon and the de-excitation of the Mn^{2+} by $\Delta m_S = -1$ involves a virtual transition at an energy $\hbar\omega_a$ for the incident radiation polarized along $\hat{z}$ and another at $\hbar\omega_b$ for scattered radiation having $\hat{\sigma}_+$ polarization. With the 7625 Å ($\hbar\omega_L$ = 1.648 eV) laser line, the "in resonance" condition is nearly fulfilled; with A and B in Eq. 18 for x = 0.05, T = 5 K and H = 60 kG, we estimate the energies of X_z and X_+, the components which move to lower energies with increasing H, to be 1.636 eV and 1.603 eV, respectively (here we use $N_o\alpha$ = 220 meV and $N_o\beta$ = -880 meV given by Gaj et al. (ref. 14)). Thus, it is clear that the "in resonance" condition is satisfied even more closely whereas the "out resonance" for ω_{LO} -

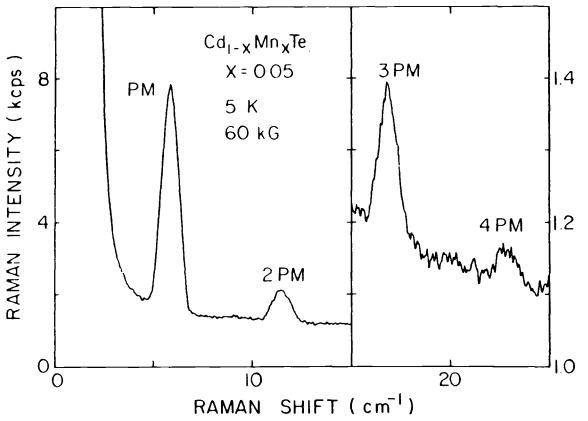

Fig. 7. The Stokes Raman lines at $n\omega_{PM}$ (n = 1,...4) resulting from Δm_S = +n spin-flip transitions in the Zeeman multiplet of the ground state of the 3d shell of Mn^{2+} in $Cd_{0.95}Mn_{0.05}Te$. Exciting wavelength λ_L = 7525 Å, power P_L = 90 mW; applied magnetic field H = 60 kG and temperature T = 5K. The spectrum for shifts greater than 15 cm^{-1} is the average of ten scans. (Peterson et al., ref. 28).

ω_{PM} can now be realized. The results in Fig. 7 show the resonantly enhanced lines at ω_{PM}, $2\omega_{PM}$, $3\omega_{PM}$, and $4\omega_{PM}$. Here we emphasize the dramatic enhancement in the intensity of the $\omega_{LO_1} - \omega_{PM}$ line as illustrated in Fig. 8 and 9. The spectra were recorded with the incident polarization along $\hat{z}$, unanalyzed scattered radiation and $\hat{k}_S \parallel \vec{H}$. The relatively broad feature at ~220 cm^{-1} is the X_+ luminescence feature attributed to the exciton component at E_x - 3A + 3B. In addition to the LO_1, $LO_1 \pm PM$, LO_2, and $LO_2 \pm PM$ lines, which have been reported before (ref. 3) two additional features with Raman shifts of

$$\omega_{LO_1} \pm 2\omega_{PM}$$

are observed. A direct consequence of the "out resonance" conditions is the pronounced

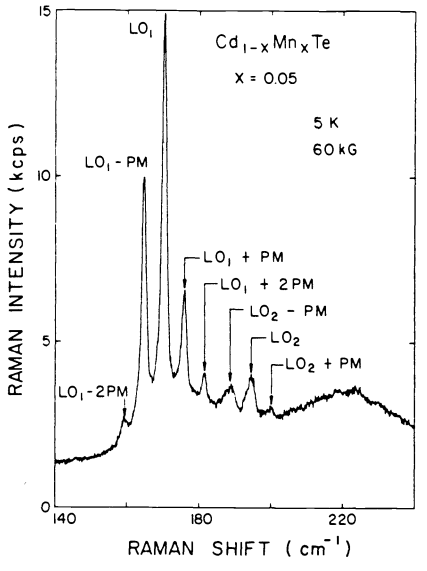

Fig. 8. The Raman spectrum of $Cd_{0.95}Mn_{0.05}Te$ in the region of the LO phonons with T = 5 K, H = 60 kG, λ_L = 7525 Å, and P_L = 30 mW. Incident light polarized along $\hat{z} \parallel \hat{H} \parallel \hat{k}_S$, and scattered light unanalyzed. (Peterson et al., ref. 28).

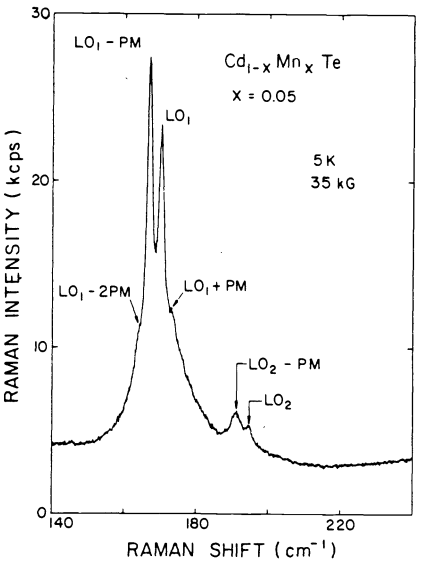

Fig. 9. The Raman spectrum of $Cd_{0.95}Mn_{0.05}Te$ in the region of the LO phonons with H = 35 kG and other conditions as in Fig. 8. (Peterson et al., ref. 28).

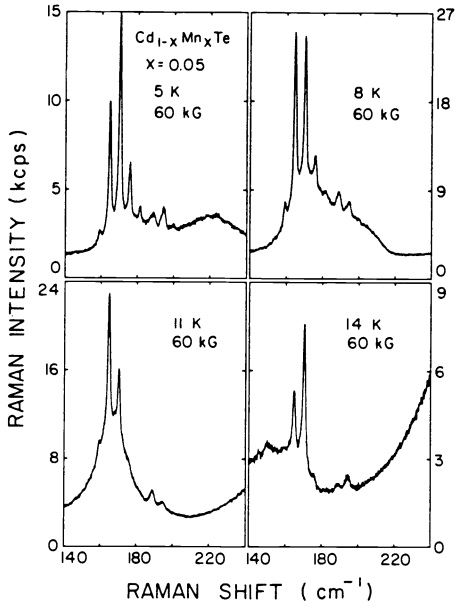

Fig. 10. Temperature variation of the resonance Raman scattering in $Cd_{0.95}Mn_{0.05}Te$ in the region of the LO phonons with H = 60 kG, and other conditions as in Fig. 8. (Peterson et al., ref. 28).

enhancement in the intensity of the LO_1 - PM line in Fig. 8 with respect to that of LO_1 + PM. In the scattering geometry and the polarization conditions used, the preferential enhancement results from the fact that the polarization of the scattered light for LO_1 + PM is $\hat{o}_-$, while that for LO_1 - PM is $\hat{o}_+$, matching that of the X_+ transition.

Under non-resonant conditions, for T = 5 K and H = 60 kG, the intensity of LO_1 + PM would be five times greater than that of LO_1 - PM, as calculated from the Boltzmann factor. This enhancement of LO_1 - PM becomes even more pronounced under exact "out resonance" achieved by decreasing the magnetic field to 35 kG and moving the X_+ luminescence feature under the LO_1 and the LO_1 - PM Raman lines; this is illustrated in Fig. 9 where the LO_1 - PM Raman line is more intense than the LO_1 line. The LO_2 - PM, LO_2, and LO_2 + PM Raman lines show similar effects as can be seen from a comparison of Figs. 8 and 9. In Fig. 10, the resonance conditions are controlled by keeping H = 60 kG but varying the temperature over the range 4.5 K - 25 K. As can be clearly seen, the resonance enhancement at T = 11 K and H = 60 kG is almost identical to that at T = 5 K and H = 35 kG. We note that the Raman shift $\omega_{LO} \pm \omega_{PM}$ is insensitive to temperature variation while the position of the Zeeman component of the exciton and, hence, the resonance conditions are strongly temperature dependent for the reasons already emphasized.

MAGNETICALLY ORDERED PHASE

As mentioned earlier, $Cd_{1-x}Mn_xTe$ exhibits a magnetically ordered low temperature phase for $x > 0.17$. The transition from the paramagnetic to the magnetically ordered phase is accompanied by the appearance of a new Raman feature at low temperatures (ref. 6) as shown in Fig. 11. Since this excitation is associated with magnetic order, it is attributed to a magnon. A distinct magnon feature was observed in $Cd_{1-x}Mn_xTe$ for the composition range $0.40 \leq x \leq 0.70$. The magnon feature is absent when the incident and the scattered polarizations are parallel and appears when they are crossed in agreement with Eq. 4 and shown in Fig. 12. This was found to be the case for several crystallographic orientations as well as for polycrystalline samples. Such a behavior, irrespective of the crystallographic orientation, is exhibited only by an excitation whose Raman tensor is antisymmetric. As the temperature is increased, the Raman shift of the magnon, ω_M, decreases, and above a characteristic Néel temperature $T_N(x)$ the feature is no longer observable. For x = 0.70, the temperature dependence of ω_M follows a Brillouin function.

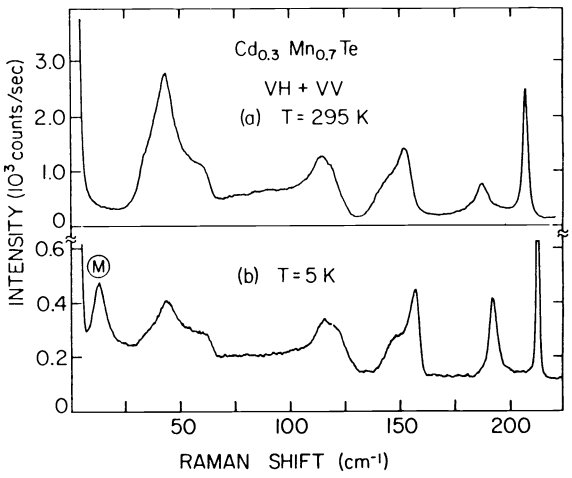

Fig. 11

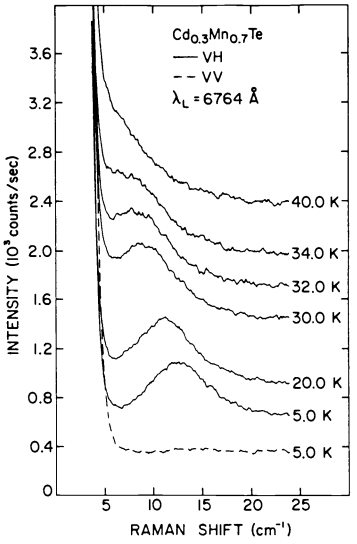

Fig. 12

Fig. 11. Raman spectra of $Cd_{0.3}Mn_{0.7}Te$ in the paramagnetic and antiferromagnetic phases; λ_L = 6764 Å. The phase transition occurs at $T_N \sim 40$ K. The scattering geometry corresponds to VH + VV. Here VH and VV denote incident light vertically polarized (V) and scattered light analyzed horizontally (H) and vertically (V), respectively, the scattering plane being horizontal. (a) T = 295 K and (b) T = 5 K. M denotes the peak due to magnon scattering. (Venugopalan et al. ref. 6).

Fig. 12. Temperature dependence of the low-frequency Raman spectrum of $Cd_{0.3}Mn_{0.7}Te$. The intensity scale refers to the VV spectrum at 5 K and successive spectra have been displaced vertically upwards for clarity. The sample temperature is indicated for each trace. The broken curve shows the VV spectrum. All the other spectra correspond to VH polarization. λ_L = 6764 Å, the exciting laser wavelength (Venugopalan et al., ref. 6).

The coordinates describing the magnons, the elementary excitations of a system of interacting magnetic dipole moments can be regarded as the Fourier components of the magnetization $\vec{M}(\vec{r},t)$. In first order Raman scattering, only the long wavelength magnons can be excited. In an antiferromagnetic system these excitations can be described by classifying the spins into those which in the state of equilibrium point in one direction and those pointing in an anti-parallel direction. This classification gives rise to magnetizations $\vec{M}_1$ and $\vec{M}_2$ where $\vec{M}_1$ is the magnetic momentum per unit volume of the spins of the first class and $\vec{M}_2$ that of the second. In equilibrium $\vec{M}_1 + \vec{M}_2 = 0$. Now, the agents responsible for the preferential orientation of a spin of type 1 are those of type 2 and conversely, the former are in a molecular field of the form $-\lambda\vec{M}_2 + \vec{H}_A^{(1)}$ where the first term, called the exchange field, is isotropic and the second points in a preferred crystallographic direction and is, thus, called the anisotropy field. The equations of motion of $\vec{M}_1$ and $\vec{M}_2$ are

$$\frac{d\vec{M}_1}{dt} = \gamma\vec{M}_1 \times (\vec{H} - \lambda\vec{M}_2 + \vec{H}_A^{(1)}) \tag{19}$$

and

$$\frac{d\vec{M}_2}{dt} = \gamma\vec{M}_2 \times [\vec{H} - \lambda\vec{M}_1 + \vec{H}_A^{(2)}] \tag{20}$$

where $\vec{H}$ is an externally applied magnetic field. Supposing, for simplicity, that $\vec{H}$ and $\vec{H}_A^{(1)} = -\vec{H}_A^{(2)}$ are parallel to a direction which we take as the z-axis, taking the exchange fields $-\lambda\vec{M}_{2,1}$ as approximately $\pm\lambda M_S = \pm H_E$ where M_S is the saturation value of M_1 we find

$$\frac{d}{dt} M_1^{\pm} = \mp i\gamma(H + H_A + H_E)M_1^{\pm} \mp i\gamma H_E M_2^{\pm} \tag{21}$$

$$\frac{d}{dt} M_2^{\pm} = \mp i\gamma(H - H_A - H_E)M_2^{\pm} \pm i\gamma H_E M_1^{\pm} \tag{22}$$

where $M_1^{\pm}$ and $M_2^{\pm}$ are $M_{1x} \pm iM_{1y}$ and $M_{2x} \pm iM_{2y}$, respectively. Equations 21 and 22 have non-trivial solutions of frequency $\omega_M^{\pm}$ given by

$$\omega_M^{\pm} = \pm\gamma H + |\gamma|(H_A^2 + 2H_A H_E)^{1/2}. \tag{23}$$

Thus when H = 0, a long wavelength magnon of frequency $|\gamma|(H_A^2 + 2H_A H_E)^{1/2}$ occurs, manifests itself in Raman scattering and is the M line in Fig. 11. The polarization features of this line are those predicted by Eq. 4 and illustrated in Fig. 12. We have here the Raman-antiferromagnetic resonance (Raman-AFMR).

We assume that H_A like H_E is proportional to the saturation values of M_1 or M_2 given by

$$M_S = (2xg\mu_B S/a^3)B_S(y), \tag{24}$$

where μ_B is the Bohr magneton, a is the lattice constant, and $B_S(y)$ is the Brillouin function with

$$y = \frac{g\mu_B S}{k_B T}(H_A + H_E) \equiv \frac{g\mu_B S}{k_B T} M_S \kappa. \tag{25}$$

The Néel temperature, T_N, is then given by

$$k_B T_N = (2x/3a^3)g^2\mu_B^2 S(S + 1)\kappa. \tag{26}$$

A numerical solution of Eq. 24 yields M_S as a function of temperature, T, and in turn the variation of ω_M with T. The best fit to the data for x = 0.70 yields T_N = 40 K.

The magnon feature in the presence of an external magnetic field of 60 kG is shown in Figs. 13a and 13c for $Cd_{1-x}Mn_xTe$, x = 0.70. The spectrum shown in Fig. 13a was recorded at T = 5 K with λ_L = 5682 Å in the $(\hat{\sigma}_-,\hat{z})$ polarization while the spectrum in Fig. 13c was observed in the $(\hat{\sigma}_+,\hat{z})$ configuration. In the following we discuss the Stokes components of these Raman features. The Raman shifts of the peaks of the features in Fig. 13 are ω_M = 8.5 cm^{-1}, and ω_{M+} = 15.5 cm^{-1}. It can be shown that a one magnon Raman line in an

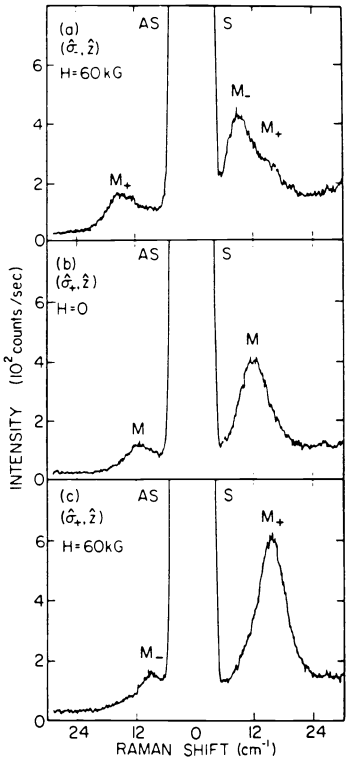

Fig. 13. Effect of the magnon feature of $Cd_{1-x}Mn_xTe$, x = 0.70, at T = 5 K with λ_L = 5682 Å. x, y, and z are along [110], [$\bar{1}$10], and [001], respectively: (a) $(\hat{\sigma}_-,\hat{z})$, H = 60 kG; (b) $(\hat{\sigma}_+,\hat{z})$, H = 0; (c) $(\hat{\sigma}_+,\hat{z})$, H = 60 kG. Owing to imperfect polarization, leakage of the fairly strong feature M_+ appears as a small shoulder in the $(\hat{\sigma}_-,\hat{z})$ configuration. (Petrou et al., ref. 3).

antiferromagnet should split into two components of equal intensity separated by $2g\mu_B H$ at T = 0 K, if $\vec{H}$ is along the anisotropy field, $\vec{H}_A$. The observed spacing between M_+ and M_- of 7 cm^{-1} for 60 kG is significantly smaller than $2g\mu_B H$ = 11 cm^{-1}. The polarization characteristics of ω_{M+} and ω_{M-} are those expected. These results are independent of the crystal orientations with respect to the applied field suggesting that H_A is small compared to the applied field.

We have described the Raman features associated with magnetic excitations appearing in the paramagnetic state as well as in the magnetically ordered phase. The exchange interaction between Mn^{2+} ions is negligible compared to $k_B T$ at high temperatures becoming more important as the temperature is lowered. It is of interest to investigate the effects of temperature on the ω_{PM} line, particularly the effect of lowering the temperature below T_N, the transition temperature characterizing the magnetically ordered phase. As the temperature is lowered, the ω_{PM} line initially broadens and then moves towards higher Raman shifts as a consequence of the increased importance of the exchange interaction. An increase in Raman shift is observed at temperatures well above $T_N \sim 40$ K. As the temperature is lowered through and below T_N, the line becomes the magnon component observed in the $(\hat{\sigma}_+, \hat{z})$ configuration.

Finally, the conclusion that the magnetic feature observed in the magnetically ordered phases is a one magnon excitation was deduced from its polarization characertistics and temperature behavior (ref. 6); this is supported by the results of Ching and Huber (ref. 15 and 16). The fact that this feature shows a splitting in the presence of a magnetic field and that the ω_{PM} line of the paramagnetic phase, clearly associated with a single ion excitation, evolves smoothly into the higher energy component of the magnon provides a strong confirmation of this interpretation. In the same spirit, one might expect a two magnon feature associated with the $2\omega_{PM}$ line; however, given the intensity of the $2\omega_{PM}$ line compared to that of the ω_{PM} line, the intensity of such a feature would preclude its observation. A two magnon feature would have symmetric polarization characteristics; such a feature has not been observed in $Cd_{1-x}Mn_xTe$.

SPIN-FLIP RAMAN SCATTERING

Since the first observations of electron spin-flip Raman scattering in the narrow band gap semiconductor InSb by Slusher et al (ref. 17) followed by that in the wide band gap semiconductor CdS by Thomas and Hopfield (ref. 18), there has been a continuing interest in this magneto-optical phenomenon. An important contribution to this field is the first demonstration of the spin-flip Raman laser by Patel and Shaw (ref. 19). The success of the InSb spin-flip Raman laser as a practical source of magnetic field tuned coherent radiation in the 5 to 15 μm spectral region (ref. 19 and 20) can be traced to the large effective g-factor of the electron, $|g^*| \gtrsim 50$. In contrast, the wider band gap II-VI semiconductors CdS, CdSe and CdTe have rather small spin splittings (ref. 18 and 21) characterized by $|g^*| \lesssim 2$, since their conduction and valence band spin-orbit interactions are small in comparison to their energy band gaps.

When detectable, spin-flip Raman scattering provides a practical means of probing the electronic structure of semiconductors, as dramatically illustrated in DMS. The large Raman shifts associated with spin-flip scattering from electrons in DMS were first observed in the narrow gap $Hg_{1-x}Mn_xTe$ by Geyer and Fan (ref. 22). The first evidence of a finite spin-splitting of the electronic level in the absence of a magnetic field was reported by Nawrocki et al. (ref. 23 and 24) in the wide gap diluted magnetic semiconductor $Cd_{1-x}Mn_xSe$. The effects of Mn concentration and the antiferromagnetic coupling among the Mn^{2+} ions on the spin-flip Raman shifts were first observed (ref. 25) in a study of $Cd_{1-x}Mn_xTe$. These

studies established the nature of Raman scattering associated with the spin-flip transitions of electrons bound to donors in DMS. The large Raman shifts depend not only on the applied magnetic field, but also on temperature and manganese concentrations. The far-infrared absorption spectra (ref. 26) of $Cd_{1-x}Mn_xSe$ also provided evidence for these spin-flip transitions.

The Raman spectra of $Cd_{1-x}Mn_xTe(Ga)$, x = 0.03, are shown in Fig. 1 for the $(\hat{\sigma}_+,\hat{z})$ and $(\hat{\sigma}_-,\hat{z})$ polarization configurations with T = 40 K and H = 60 kG. The two Stokes features labeled 'PM' and 'SF' are present only in $(\hat{\sigma}_+,\hat{z})$, while the corresponding anti-Stokes features appear only in the $(\hat{\sigma}_-,\hat{z})$ configuration. The observed width of the 'PM' line is instrument limited, while that of the spin-flip transitions is $\sim$3 cm^{-1}.

The 'SF' feature of Fig. 1 is attributed to spin-flip Raman scattering from electrons bound to gallium donors. It has the same polarization characteristics as those of the 'PM' line appearing (ref. 25) in the $(\hat{\sigma}_+,\hat{z})$ or $(\hat{z},\hat{\sigma}_-)$ polarizations for Stokes scattering and in $(\hat{\sigma}_-,\hat{z})$ or $(\hat{z},\hat{\sigma}_+)$ for anti-Stokes. As illustrated in Fig. 14, the peak Raman shift of this spin-flip feature exhibits a strong dependence on both temperature and magnetic field. The primary source of the spin splitting of the electronic level is the exchange coupling with the Mn^{2+} ions with the Zeeman effect making a relatively small contribution. Hence, the Raman shift should be approximately proportional to the magnetization of the Mn^{2+} ion system, which amplifies the effect of the magnetic field on the electron. As can be seen in Fig. 14, a finite Raman shift is observed for zero magnetic field. This effect is attributed by Dietl and Spalek (ref. 27) to the "bound magnetic polaron (BMP)": The electron localized on a donor in a diluted magnetic crystal polarizes the magnetic ions within its orbit, creating a spin cloud that exhibits a net magnetic moment. Electron spin-flip under such conditions require the expenditure of energy even when $\vec{H} = 0$.

The spin-flip Raman shifts for $Cd_{1-x}Mn_xTe$ at T = 1.8 K are shown in Fig. 15 as a function of magnetic field and composition. The results for x = 0.01 show the saturation behavior characteristic of the paramagnetic phase. As the Mn concentration is increased to x = 0.03 and x = 0.05, the Raman shifts increase and the effects of saturation are still clearly

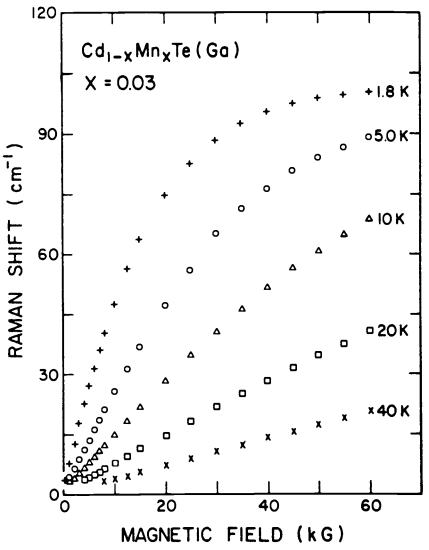

Fig. 14. Magnetic field and temperature dependence of the Raman shift associated with the spin-flip of electrons bound to donors in $Cd_{1-x}Mn_xTe(Ga)$, x = 0.03 (Peterson et al., ref. 29).

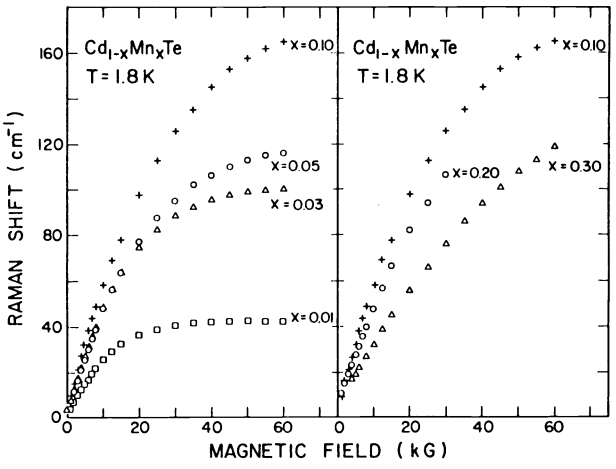

Fig. 15. Magnetic field and composition dependence of the peak spin-flip Raman shift in the $Cd_{1-x}Mn_xTe$ samples at T = 1.8 K (Peterson et al., ref. 29).

evident, but less pronounced. For x = 0.10, the deviation from the paramagnetic behavior is quite evident. For H = 60 kG, the Raman shift for x = 0.10 is only four times that for x = 0.01. As x exceeds 0.10, the Raman shifts for a given field actually decrease; note that the shfits for the x = 0.20 sample lie below those for the x = 0.10 sample. And the Raman shifts for the $Cd_{1-x}Mn_xTe(Ga)$, x = 0.30, sample are significantly smaller than those for the x = 0.10 and x = 0.20 samples. These trends have their origin in the decrease of the mean magnetic field due to the increasing antiferromagnetic pairing of Mn^{2+} neighbors.

Acknowledgements

The support from the National Science Foundation during the preparation of this paper is gratefully acknowledged (Grant Nos. DMR-84-03325 and DMR-85-20866).

REFERENCES

1. L.D. Landau and E.M. Lifshitz (1960), Electrodynamics of Continuous Media, Pergamon Press, Oxford, 331 (1960).
2. J. Lambe and C. Kikuchi, Phys. Rev., 119, 1256 (1960).
3. A. Petrou, D.L. Peterson, S. Venugopalan, R.R. Galazka, A.K. Ramdas, and S. Rodriguez, Phys. Rev. B, 27, 3471 (1983).
4. P.A. Fleury and R. Loudon, Phys. Rev., 166, 514 (1968).
5. W. Hayes and R. Loudon, Scattering of Light by Crystals, Wiley, New York, (1978).
6. S. Venugopalan, A. Petrou, R.R. Galazka, A.K. Ramdas, and S. Rodriguez, Phys. Rev. B, 25, 2681 (1982).
7. R. Loudon, Proc. Roy. Soc., London, A275, 218 (1963).
8. R. Loudon, Advances in Physics, 13, 423 (1964).
9. A.S. Barker, Jr. and R. Loudon, Rev. Mod. Phys., 44, 18 (1972).
10. A. Twardowski, M. Nawrocki and J. Ginter, Phys. Stat. Sol. (b), 96, 497 (1979).
11. R. Planel, J. Gaj, and C. Benoit a la Guillaume, J. Phys. (Paris) Colloq., 41, C5-39 (1980).
12. Y.R. Lee and A.K. Ramdas, Solid State Commun., 51, 861 (1984).
13. S.M. Ryabchenko, O.V. Terletskii, I.B. Nizetskaya, and G.S. Oleinik, Fiz. Tekh. Poluprovodn., 15, 2314 (1981), [Sov. Phys. Semicond.), 15, 1345 (1981)].
14. J.A. Gaj, R. Planel, and G. Fishman, Solid State Commun., 29, 435 (1979).
15. W.Y. Ching and D.L. Huber, Phys. Rev. B, 25, 5761 (1982).
16. W.Y. Ching and D.L. Huber, Phys. Rev. B, 25, 6164 (1982).
17. R.E. Slusher, C.K.N. Patel, and P.A. Fleury, Phys. Rev. Lett., 18, 77 (1967).
18. D.G. Thomas and J.J. Hopfield, Phys. Rev., 175, 1021 (1968).
19. C.K.N. Patel and E.D. Shaw, Phys. Rev. Lett., 24, 451 (1970).
20. A. Mooradian, S.R.J. Brueck, and F.A. Blum, Appl. Phys. Lett., 17, 481 (1970).
21. T.W. Walker, C.W. Litton, D.C. Reynolds, T.C. Collins, W.A. Wallace, J.H. Gorrell, and K.C. Jungling, Proceedings of the XI International Conference on the Physics of Semiconductors, Warsaw, 1972, Elsevier, New York, 376 (1972).
22. F.F. Geyer and H.Y. Fan, IEEE J. Quantum Electron., QE-16, 1365 (1980).
23. M. Nawrocki, R. Planel, G. Fishman, and R.R. Galazka, Proceedings of the XV International Conference on the Physics of Semiconductors, (S. Tanaka and Y. Toyozawa, eds.), J. Phys Soc. Jpn. Suppl., A49, 823 (1980).
24. M. Nawrocki, R. Planel, G. Fishman, and R.R. Galazka, Phys. Rev. Lett., 46, 735 (1981).
25. D.L. Peterson, A. Petrou, M. Dutta, A.K. Ramdas, and S. Rodriguez, Solid State Commun., 43, 667 (1982).
26. M. Dobrowolska, H.D. Drew, J.K. Furdyna, T. Ichiguchi, A. Witowski, and P.A. Wolff, Phys. Rev. Lett., 49, 845 (1982).
27. T. Dietl and J. Spalek, Phys. Rev. B, 28, 1548 (1983).
28. D.L. Peterson, D.U. Bartholomew, A.K. Ramdas, and S. Rodriguez, Phys. Rev. B, 31, 7932 (1982).
29. D.L. Peterson, D.U. Bartholomew, U. Debska, A.K. Ramdas, and S. Rodriguez, Phys. Rev. B, 32, 323 (1985).